Advances in Materials
2018; 7(4): 118-127
http://www.sciencepublishinggroup.com/j/am
doi: 10.11648/j.am.20180704.14
ISSN: 2327-2503 (Print); ISSN: 2327-252X (Online)

Formulation of Aqueous Dispersions of PEKK by a Quantitative Structure Property Relationship Approach and Application to Thermoplastic Sizing on Carbon Fibers

Mike Alexandre[1, 2, 3], Emile Perez[2], Colette Lacabanne[3], Eric Dantras[3], Sophie Franceschi[3], Damien Coudeyre[1], Jean-Christophe Garrigues[2, *]

[1]Institute of Technology Antoine de Saint Exupéry, Toulouse, France

[2]Interactions Moléculaires Réactivité Chimique et Photochimique Laboratory, Toulouse University, Toulouse, France

[3]Centre Interuniversitaire de Recherche et d'Ingénierie des Matériaux, Toulouse University, Toulouse, France

Email address:

mike.alexandre@irt-saintexupery.com (M. Alexandre), damien.coudeyre@irt-saintexupery.com (D. Coudeyre), colette.lacabanne@univ-tlse3.fr (C. Lacabanne), eric.dantras@univ-tlse3.fr (E. Dantras), sfrances@chimie.ups-tlse.fr (S. Franceschi), perez@chimie.ups-tlse.fr (E. Perez), jean-christophe.garrigues@chimie.ups-tlse.fr (J. C. Garrigues)

[*]Corresponding author

To cite this article:

Mike Alexandre, Emile Perez, Colette Lacabanne, Eric Dantras, Sophie Franceschi, Damien Coudeyre, Jean-Christophe Garrigues. Formulation of Aqueous Dispersions of PEKK by a Quantitative Structure Property Relationship Approach and Application to Thermoplastic Sizing on Carbon Fibers. *Advances in Materials*. Vol. 7, No. 4, 2018, pp. 118-127. doi: 10.11648/j.am.20180704.14

Received: November 6, 2018; **Accepted**: November 26, 2018; **Published**: December 18, 2018

Abstract: The development of formulations for thermoplastic sizing on carbon fibers requires water dispersions of small polymer particles (< 20 µm). PolyEtherKetoneKetone (PEKK) is a high-performance polymer used as a matrix in Carbon Fiber Reinforced Polymers (CFRP) or as a sizing agent. To limit the formulation steps and the use of organic solvents, the sonofragmentation process can be used to deagglomerate polymers, directly in the final aqueous formulation. The sonofragmentation process is controlled by multiple parameters and, in order to identify the key parameters, a quantitative structure property relationship (QSPR) study was performed using artificial neural networks (ANN). The 40 formulations of this study were characterized with the aim of quantifying the sonofragmentation effect. Various physicochemical techniques were used: Photon Correlation Spectroscopy (PCS), destabilization velocity of the dispersions by analytical centrifugation, and scanning electron microscopy. The results obtained showed that only two parameters (mass concentration of surfactant and duration of sonication) had a notable effect on the sonofragmentation process. By controlling these two parameters, it was possible to define a design space in the stability domain of the formulations and to calculate a sonofragmentation efficiency (ϕ) for four singular zones. Image analysis showed that the sonofragmentation process was accompanied by an increase in the number of particles with Particle size (Ps) < 20 µm. In optimized aqueous formulations, the majority of particles should have Ps < 20 µm.

Keywords: Processing Technologies, Quantitative Structure Property Relationship, Aqueous Formulations, Polymer Composites, Thermoplastic Sizing, PEKK, Artificial Neural Network

1. Introduction

Coating by high-performance polymers is being increasingly used to protect chemically and thermally sensitive materials [1–3]. Thermoplastic polymers are often used to coat materials at high temperature, and among them PolyEtherEtherKetone (PEEK) and PolyEtherKetoneKetone (PEKK) are polymers of choice [4, 5]. The latter is largely used in the automotive and aerospace industries [6, 7] and has very good chemical and thermal resistance, but its high melting temperature (300-360°C) makes it unsuitable for coating very sensitive materials. In this context, waterborne coatings, such as latexes, could provide a very interesting alternative to hot coating, [8–10] and the use of organic solvents (toxicity, flammability). Unfortunately, the synthesis

of PEKK does not lend itself the direct preparation of stable latexes and, for a waterborne coating, this polymer must be subdivided and dispersed in water.

Other uses of polymer coating exist, especially in the field of aeronautics to enhance the mechanical performance of Carbon Fiber Reinforced Polymers (CFRPs) by improving the fiber/matrix interface. This coating is called sizing.

Sizing is an aqueous or organic dispersion of polymer particles deposited on the surface of the carbon fibers. However, in order to promote its action, its particle size must be compatible with the diameter of the filaments constituting the fiber.

At present, many sizings are organic formulations or involve an organic solvent during the production process, [11–16] and the development of green sizing formulations requires stabilized water dispersions.

The design of materials with novel properties often requires the fine subdivision of solids (organic or mineral). The final properties of the product depend on the size of the particles and their distribution [17]. For example, size reduction may improve the stability and reactivity of colloidal dispersions [18]. Fine particles can be produced by "bottom-up" processing, in which the material is synthesized, aggregated or condensed, [19–21] or by a "top-down" approach, in which large particles are reduced by grinding or milling [22]. Size reduction to produce small particles of solid materials can be carried out by mechanical means using dry or wet milling techniques, including ball milling, jet milling, media milling, and homogenization [23–25]. In addition to these mechanical processes, the use of ultrasonic milling (sonofragmentation using ultrasonic devices) to deagglomerate solids into liquids is becoming increasingly common [26–28]. The mechanical stress generated by ultrasonic cavitation breaks the agglomerates apart and can erode the particles to much smaller sizes [29]. Generally, to avoid reagglomeration, the sonofragmentation is assisted by dispersing agents such as surfactants or polymers [30, 31]. Concerning the solid to be subdivided, there are many more examples of minerals and small organic molecules than of polymers.

In this work, a commercially available PEKK was chosen with a Terephthalic/Isophthalic ratio [32] T/I = 60/40, that was compared with corresponding extractible fractions that might be most easily obtained as small particles (PEKK oligomers). Sonofragmentation could be a promising method for reducing and controlling their size. The parameters controlling the sonofragmentation process have been studied [33]. Temperature, sonication power and duration play important roles in particle breakage. For more complex formulations, requiring the addition of surfactant to stabilize the particles, the number of parameters to be controlled becomes very large. To optimize the sonofragmentation in these cases, it is necessary to understand the relationships between each parameter that influences the process and the properties of the treated polymer. Quantitative structure property relationship (QSPR) studies have shown their utility in revealing the quantitative relation connecting the structure of polymers to their properties [34]. In this study, a QSPR method was used in association with an artificial neural network (ANN) to identify the parameters involved in the process. From these key parameters, an experimental design space optimizing the sonofragmentation process for PEKK polymer was explored. To evaluate the properties of the polymer particles, two physicochemical methods were compared: photon correlation spectroscopy and destabilization velocity of the dispersions.

The formulation process developed provided an optimized formulation of sizing agent of low molecular weight (PEKK oligomers). Subsequently, CFRPs with sized carbon fibers were compared to a unsized carbon fiber reinforced composite. Their fracture surfaces were observed by SEM in order to compare the efficiency of the sizing through the fiber/matrix interface.

2. Material and Methods

2.1. Materials for Sonofragmentation Process

2.1.1. PEKK Extractible Fraction Fragmentation

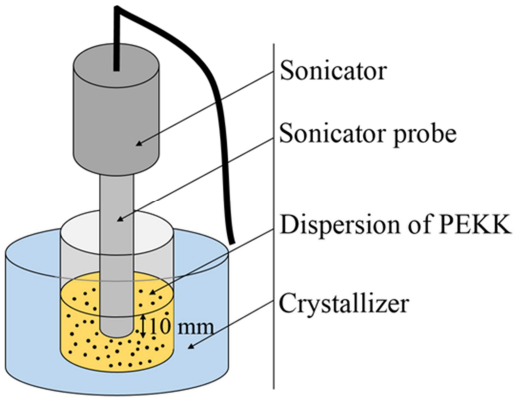

Figure 1. *Scheme of the experimental sonofragmentation setup.*

For this study, 40 experiments were carried out. Every aqueous dispersion (deionized water) contained 0.4 g of PEKK extractible fraction (Arkema, France) and cetyltrimethylammoniun chloride (CTAC) surfactant (Sigma-Aldrich, USA). Sonofragmentation was used to disperse and to fragment the PEKK extractible fraction or (PEKK oligomer), according to 7 controlled experimental parameters: volume of liquid (V), mass concentration of surfactant (C_{CTAC}), duration of sonication (t), percentage of active cycles (A), dissipation of heat (D_{HEAT}), and intensity of ultrasound (I). To investigate the effect of liquid oxygenation (OX_{effect}), the deionized water was gas saturated by bubbling O_2 (Alpha gaz 1, Airliquide, France) through it for 24 h, or the deionized water was left in its native, unsaturated state. Figure 1 shows the experimental setup used for all water dispersions. A Bioblock Scientific sonicator (Fisher Bioblock Scientific, France, model: 72402) was used at a frequency of 20 kHz, with 600 W input power, and a probe 13 mm in diameter. During the sonofragmentation, the probe was immersed in the dispersion to a depth of 10 mm.

2.1.2. PEKK Polymer Fragmentation

PEKK (Arkema, France) with a Terephthalic/Isophthalic ratio T/I = 60/40 and particle size of 20 µm was used. Every aqueous dispersion was made of 0.4 g of PEKK dispersed in 10 ml of native deionized water. The dispersion system was similar to that described above (Figure 1). The sonofragmentation conditions applied for this study were the following: A = 50 %, without D_{HEAT} and I = 4. Every sample was defined by two parameters: C_{CTAC}, between 0 and 20 wt. %; and t, between 0 and 45 min.

2.2. Photon Correlation Spectroscopy Analysis

The mean diameter of the particles (*Ps*) and the distribution size index (*Ds*) were determined at 25°C by Photon Correlation Spectroscopy (PCS) at a scattering angle of 173° (Zetasizer® Nano ZS, Malvern PCS Instruments, UK). Every dispersion was measured 3 times for 10 runs of 10 seconds.

2.3. Scanning Electron Microscopy for Characterization of PEKK Particles

The microstructure of the dispersion was observed by scanning electron microscopy (SEM) (FEG SEM JEOL JSM 7800F-Prime). The micrographs obtained were used for additional estimation of the particle size, morphology and fragmentation efficiency (ϕ) calculation. ϕ was calculated on an average of 100 objects per image defined by Image J software (Image J 1.50e, National Institutes of Health, USA) as the number of particles with $Ps < 20$ µm on the 100 measured objects (%). Cryocut observations were observed according to the same protocol.

2.4. Destabilization of the Dispersions by Analytical Centrifugation

The destabilization velocity of the dispersions (v) expressed in %/min was determined by analytical centrifugation (LUMiFuge® 110 Stability Analyser, LUM GmbH, Germany).

The sample was subjected to centrifugation (200 rpm to 4000 rpm) leading to an accelerated destabilization of the dispersion at 25°C. LUMiFuge® operations is analyzed evolution of sedimentation profile of dispersion sample submitted a centrifugation cycle, depending on the time.

2.4.1. PEKK Extractible Fraction

Before analytical centrifugation analysis, all the PEKK extractible fraction dispersions were re-dispersed using a shaker table (Ika HS 260, Germany) for 4 h at 270 oscillations/min. Every sample was analyzed by LUMiFuge® according to the following method: 4000 rpm, 255 profiles, 10 s/profile at 25°C.

2.4.2. PEKK Polymer

The PEKK dispersions were analyzed by LUMiFuge® using: 2000 rpm, 100 profiles, 10 s/profile at 25°C.

2.5. Implementation of CFRP

Carbon fiber was sized by dip-coating in thermoplastic sizing of PEKK oligomer. The carbon fiber sized was impregnated by PEKK polymer and the composite was implemented at 360°C for 15 min. Cryocut observations were obtained by freezing and cutting the CFRP material in liquid nitrogen (5 min) before SEM.

3. QSPR Theory and Utilization of Neural Network

The bases of QSPR studies were laid down in a joint work by Hammett [35], Taft [36], Hansch and Fujita [37], and Free and Wilson [38]. QSPR modelling consists of constructing predictive models of properties as functions of structural and reaction or physicochemical information from a compound library or experiments. Broderick and Rajan [39], have shown an example of the utilization of QSPR in development incorporating the impact of data uncertainty, which allows new databases to be developed rapidly.

The development of a QSPR model typically comprises two steps: (1) description of molecular structures or controlled reaction parameters and (2) multivariate or ANN analysis to correlate molecular descriptors or controlled parameters with observed properties. The first application of ANN in the search for correlations between molecular structure and biological property was achieved by Hiller et al. [40], using perceptron to classify substituted dioxanes as active or inactive according to their physiological activity. The algorithms generally used in applications of ANN in quantitative structure activity relationship (QSAR) or QSPR studies are characterized by a wide variety of neural network architectures and different approaches to represent chemical structures, parameters or properties. The multilayer feed forward ANN associated with a back propagation algorithm are generally used in QSAR and QSPR studies.

The back propagation algorithm was originally proposed by Rumelhart et al. in 1986 [41]. An ANN approach mimics the operation of the human brain by using interconnected processing elements to rule on relationships between experimental and calculated data. The "neurons" are connected processing elements. The data are exchanged using a transfer function modulated by variable weights.

Every neuron performs three operations on all the data:

(1) Activation by transformation of the sum of all inputs into a function (linear or sigmoid) producing an output value.

(2) Weighting, with the determination of a multiplication factor for each input.

(3) Summation: summing of weighted inputs.

The multi-layer perceptron is generally composed of three independent layers: the input, hidden and output layers [42, 43]. This structure, named Hopfield's network, is commonly used for prediction and validation processes.

In the input layer, each neuron is connected to an experimental parameter of the system under study. Information is "fed forward" to the hidden and output neurons [44]. In a QSPR study, the output neuron is associated with

physicochemical properties. The hidden layer acts as an intermediary for the operations of summation and activation. Generally, the number of hidden neurons is half the number of input neurons.

SNNS (Stuttgart Neural Network Simulator) v4.2, software developed at the University of Stuttgart, Germany, was used to model the relationships between sonofragmentation controlled parameters and the characteristics of the polymer particles obtained in this study, through a back propagation algorithm. SNNS software has been successfully used in the prediction of trihalomethane concentrations for drinking water [45], simulation of neutron scattering spectra [46], elimination of dual radionuclide $^{99m}Tc/^{123}I$ images crosstalk [47], optimization of optical fiber sensor cross-sensitivity [48], and optimization of the free radical scavenging properties of thiol and amino thiol derivatives [49]. The optimization of the parameters controlling the particle size, dispersity and stability of formulations used for the development of fiber sizing for composite material design was also performed with an ANN QSPR study.

4. Results and Discussion

4.1. Optimization by ANN with PEKK Extractible Fraction

The datasets used in this study were organized starting from all 7 parameters that influenced the sonofragmentation process, as described in Table 1. The data were coded and normalized (Table 1), before being organized as input parameters in 21 different datasets connected with 3 experimental physicochemical parameters: particle size (Ps), distribution size (Ds) or destabilization velocity (v) (Table 2). The dataset files were then used with the different ANNs, (Table 3). These 21 datasets were created by operator depending on statistical weight obtained by neural network: NN0A, NN0B and NN0C for samples before destabilization velocity analysis. NN0D and NN0E after destabilization velocity analysis.

Table 1. *Details of input parameters used in the QSPR study, showing parameter type, experimental range level and coded values.*

Parameter type	Abbreviation	Range level: Coded level
Volume of liquid (ml)	V	10:0.5; 15:0.75; 20:1
Mass concentration	C_{CTAC}	0: 0; 1:0.05; 2:0.1; 5:0.25;
of surfactant (wt. %)	t	10:0.5; 20:1
Duration of sonication (min)	A	15:0.5; 30:1
Percentage of activity (%)	OX_{effect}	20:0.25; 50:0.625; 80:1
Liquid oxygenation	D_{HEAT}	With: 1; Without: 0
Heat dissipation	I	With: 1; Without: 0

After the sonofragmentation process, every of the 40 dispersions was analyzed by PCS, measuring two output parameters: distribution size (Ds) and particle size (Ps). In a first step, an ANN without a hidden layer was used (NN0A, Table 3) with dataset 1 (Table 2), in order to obtain the weight as an absolute value for each of the 7 controlled parameters according to the learning cycle. By modifying these weights, NN0A calculated the most important input parameters for Ds or Ps. For Ds, key parameters were not really defined because their statistical weights were lower than 1 (Table 4). For Ps, C_{CTAC} (6.27) and I (3.15) were the key parameters with the greatest weight values, after 15 000 learning cycles (Table 4).

In a second step, for Ps, we carried out a cross-validation process to evaluate the validity of the different ANNs constructed with all the input controlled parameters (NNA5, Table 3), or the ANN constructed with the 2 key parameters C_{CTAC} and I (NNA8, Table 3). To confirm the key parameters, NNA6, containing the 5 parameters of weight > 1, and NNA7, containing C_{CTAC} and V, were built (Table 3). For all NNAx, where x is the NN number (Table 3), a training set was prepared with 39 experiments having the desired number of inputs. The experiment that was not present in the training set was used as a validation set. This procedure was repeated until the 40 experiments had been calculated in the validation set. After this cross-validation procedure, it was possible to correlate the predicted Ps value (nm) with the experimental value for the 40 experiments.

For all the validation agreement plots corresponding to NNAx, the correlation coefficient values (R^2) were lower than 0.5, indicating an absence of linear relation and invalidating the models. There are two hypotheses that may explain why the model with particle size measurements proved invalid. The first reason could be a high sedimentation of the larger particles before PCS analysis and the second could be that the stable suspended particles had a size outside the measurement range for the PCS analysis.

This Ps value corresponds to the upper limit of detection of the device and small particles were mixed with aggregates. Ps was determined from fluctuations in scattered light intensity due to Brownian movement of the particles [50]. Dust particles or small amounts of large aggregates could invalidate the size determination if the main component exhibited a smaller size [51]. Before sonofragmentation, PCS results for the different samples were 0. For ANN, the value 0 is very complex to interpret: an absence of particles in the formulation or Ps equal to or larger than 10 µm. This suggests that PCS analysis is irrelevant in our case.

Table 2. *Details of input parameters used in the QSPR study.*

Data set	Number of input parameters	Input parameters	Output parameter
1	7	V, C_{CTAC}, t, A, OX_{effect}, D_{HEAT}, I	Ds
2	7	V, C_{CTAC}, t, A, OX_{effect}, D_{HEAT}, I	Ps
3	7	V, C_{CTAC}, t, A, OX_{effect}, D_{HEAT}, I	v
4	3	A, OX_{effect}, D_{HEAT}	Ds
5	2	A, D_{HEAT}	Ds
6	2	OX_{effect}, D_{HEAT}	Ds
7	5	V, C_{CTAC}, OX_{effect}, D_{HEAT}, I	Ps
8	2	V, C_{CTAC}	Ps
9	2	C_{CTAC}, I	Ps
10	4	V, C_{CTAC}, t, I	v
11	3	V, C_{CTAC}, t	v
12	3	C_{CTAC}, t, I	v
13	2	C_{CTAC}, t	v
14	2	C_{CTAC}, t	Ds
15	4	V, C_{CTAC}, A, I	Ps
16	3	V, C_{CTAC}, A	Ps
17	3	V, C_{CTAC}, I	Ps
18	3	V, A, I	Ps
19	2	V, C_{CTAC}	Ps
20	2	V, A	Ps
21	2	V, I	Ps

Table 3. *Architecture of ANNs with the datasets used, the associated number and type of nodes, and the type of output parameter.*

Neural Network	Data set used (Table 2)	Number of parameters			Type of output parameter
		input	hidden	output	
NN0A	1	7	0	1	*Ds*
NN0B	2	7	0	1	*Ps*
NN0C	3	7	0	1	*v*
NN0D	1	7	0	1	*Ds*
NN0E	2	7	0	1	*Ps*
NNA1	1	7	4	1	*Ds*
NNA2	4	3	2	1	*Ds*
NNA3	5	2	2	1	*Ds*
NNA4	6	2	2	1	*Ds*
NNA5	2	7	4	1	*Ps*
NNA6	7	5	3	1	*Ps*
NNA7	8	2	2	1	*Ps*
NNA8	9	2	2	1	*Ps*
NNL1	3	7	4	1	*v*
NNL2	10	4	3	1	*v*
NNL3	11	3	2	1	*v*
NNL4	12	3	2	1	*v*
NNL5	13	2	2	1	*v*
NNB1	1	7	4	1	*Ds*
NNB2	14	2	2	1	*Ds*
NNB3	2	7	4	1	*Ps*
NNB4	15	4	3	1	*Ps*
NNB5	16	3	2	1	*Ps*
NNB6	17	3	2	1	*Ps*
NNB7	18	3	2	1	*Ps*
NNB8	19	2	2	1	*Ps*
NNB9	20	2	2	1	*Ps*
NNB10	21	2	2	1	*Ps*

Table 4. *Statistical weights in absolute value before analytical centrifugation for each output parameter after 15 000 learning cycles for NN0A (Ds) and NN0B (Ps).*

Input parameters	Output parameter measured in direct experiments	
	Distribution size (Ds)	Particle size (Ps)
V	0.21	2.00
C_{CTAC}	0.03	6.27
t	0	0.71
A	0.78	0.22
OX_{effect}	0.90	1.40
D_{HEAT}	0.81	1.41
I	0.39	3.15

In order to obtain a relevant output parameter for every sample, an analytical centrifugation was used to study the destabilization velocity of the dispersions. This analysis allowed the v to be determined according to the centrifugation speed, the number of profiles, the interval value between the profiles and the temperature of the sample. Then, the statistical weight of the 7 input parameters controlling sonofragmentation was determined according to a QSPR procedure with NN0C (Table 3). It appeared that 2 parameters had a high weight: C_{CTAC}: 4.49 and t: 3.19 (Table 6). After destabilization velocity analysis, the supernatant of the sample was analyzed

by PCS for Ps and Ds determination. The statistical weight of each of the 7 input parameters controlling sonofragmentation was determined with NN0D and NN0E (Table 3). C_{CTAC}: 4.55 and t: 3.19 were the 2 parameters with the strongest weight for Ds. For Ps, all the parameters had a weight close to 1 (Table 6).

This study shows that velocity v is an important output parameter for the comparison of sonofragmentation samples. It is possible to match a low velocity with small or more stable particles in the suspension. To validate the 2 key parameters linked to v, a cross-validation process was achieved with NNL5 (Table 3). R^2 for this plot was 0.58, suggesting a trend for this model (Figure 2) and showing the influence of C_{CTAC} and t in the control of the destabilization velocity of the dispersions, after sonofragmentation.

For the 2 key parameters, C_{CTAC} and t, linked to Ds of the supernatant after centrifugation, a cross-validation process was achieved with NNB2. For Ps, different ANNs were built: from NNB4 to NNB10 with the 7, 4, 3 or 2 parameters of highest weights (Table 4). The performances of these ANN were compared by calculating the sum of the errors between the experimental value and the calculated value, after the learning cycle, for the 40 samples (Table 5). NNB8 showed the smallest total error (Table 5) with C_{CTAC} and t linked to Ps.

Table 5. *Sum of errors for each ANN.*

Neural networks	Sum of errors
NNA1	3.63
NNA2	3.01
NNA3	4.69
NNA4	3.23
NNA5	7372.72
NNA6	6763.19
NNA7	4948.20
NNA8	5498.39
NNL1	611.38
NNL2	583.68
NNL3	536.24
NNL4	560.77
NNL5	526.84
NNB1	3.35
NNB2	2.44
NNB3	3200.46
NNB4	3208.31
NNB5	3092.57
NNB6	3020.82
NNB7	3971.49
NNB8	2934.74
NNB9	3846.85
NNB10	3734.84

Validation agreement plots for Ds and Ps in the supernatant were plotted for NNB2 and NNB8. The only model that could be validated was NNB2, with a linear coefficient R^2NNB2 = 0.8. For this model, C_{CTAC} and t were linked to Ds of the supernatant after centrifugation.

Table 6. *Statistical weights in absolute values after analytical centrifugation for each output parameter after 15 000 learning cycles for NN0C (v), NN0D (Ds) and NN0E (Ps).*

	Output parameter measured in direct experiments		
Input parameters	Velocity (v)	Distribution size of supernatant (Ds)	Particle size of supernatant (Ps)
V	1.33	0.23	1.09
C_{CTAC}	4.49	4.55	0.85
t	3.19	3.19	0.31
A	0.58	0.09	0.83
OX_{effect}	0.40	0.23	0.39
D_{HEAT}	0.23	0	0.45
I	1.07	0.06	0.80

In order to confirm the model, an experimental design space was defined, with the 2 key parameters, C_{CTAC} and t, identified as controlling the performance of sonofragmentation by the destabilization velocity study of the dispersions. In order to

check that the model was not related to one particular polymer, a suspension of PEKK was used.

4.2. Validation of Model with PEKK Polymer

Every PEKK formulation was dispersed and analyzed by destabilization centrifugation. The design space representing v related to C_{CTAC} and t was plotted (Figure 3). This design space contains 4 singular zones: A without CTAC for t values from 0 to 45 min; B with 2 wt.% for C_{CTAC} and sonofragmentation duration of 30 min; C with 20 wt.% for C_{CTAC} and t = 30 min; and D with 5 wt.% for C_{CTAC} and without sonofragmentation. For B, C and D, CTAC concentration is higher than its critical micelle concentration (CMC). The CMC for CTAC has been reported to be 1.3 mM [52], whereas the molar concentration is 62.5 mM for B, 625 mM for C and 156 mM for D.

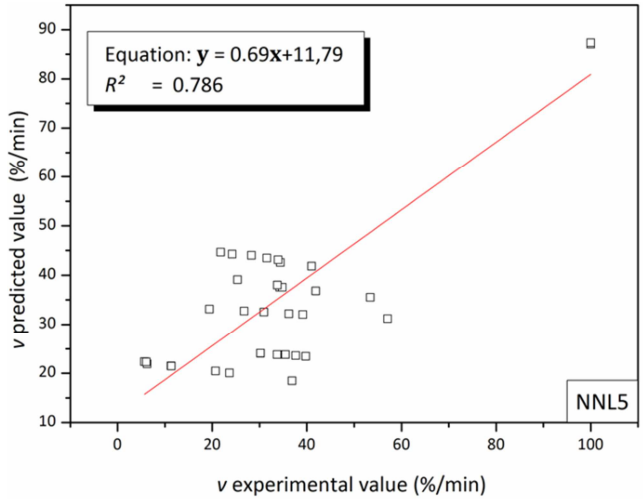

Figure 2. *Validation agreement plot for v associated with C_{CTAC}, t (NNL5) after analytical centrifugation analysis. The line corresponds to perfect prediction and squares to values predicted by ANN.*

B and C correspond to minima of v whereas D corresponds to a zone where the sonofragmentation was not carried out. For A, the absence of surfactant meant that the particles were not stabilized in the formulation, explaining the very low value measured for v which was thus considered out of the limits of measurement. These 4 zones were studied by scanning electron microscopy (Figure 4). In order to interpret the SEM observations, the particles were counted for ϕ calculation and then classified according to the histogram on Figure 5. For D without sonofragmentation, the majority of particles had Ps ranging from 20 to 30 µm.

The process of sonofragmentation produced smaller particles, but the analysis also showed particles from 30 to 100 µm, which were very quickly destabilized by the analytical centrifugation without surfactant, explaining the very low destabilization velocity observed on the design space for A (Figure 3). For B and C, the majority of particles ranged from 5 to 15 µm, and particles < 5 µm were also found for B. This classification associated with the efficiency determination of sonofragmentation, showed that B (ϕ_B = 75 %) and C (ϕ_C = 61 %) corresponded to domains with high levels of sonofragmentation, as observed on the design space (Figure 3).

A (ϕ_A = 53 %) corresponds to a domain with poor sonofragmentation yield compared to D (ϕ_D = 38 %), where sonofragmentation was not carried out. These results related to scanning electron microscopy observations are in agreement with the results obtained in the destabilization study of the dispersions by analytical centrifugation of all the samples. In the presence of surfactant, a low value of ϕ is connected with a large number of particles having Ps < 20 µm and with a high size distribution index.

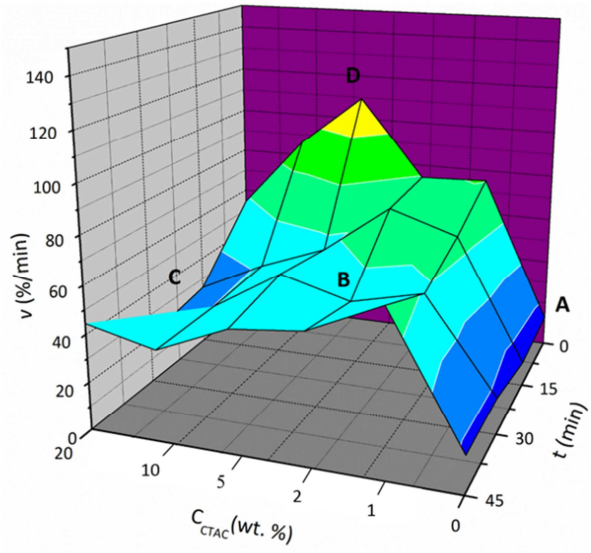

Figure 3. *Design space representing v related to C_{CTAC} and t for PEKK aqueous dispersion.*

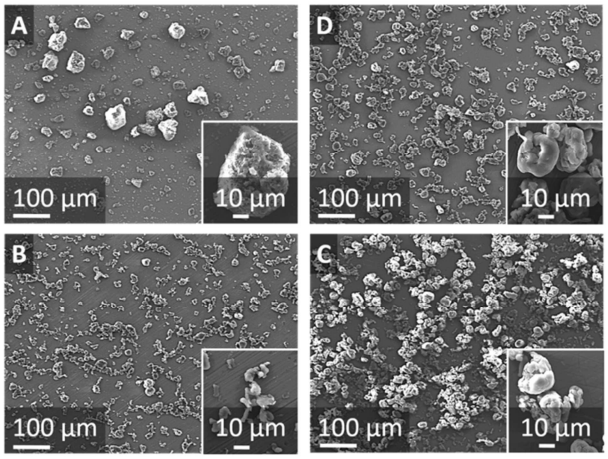

Figure 4. *Scanning electron microscopy of PEKK for the 4 typical zones of the design space of the sonofragmentation process: (A) without C_{CTAC}; (B) with 2 wt.% for C_{CTAC} and t = 30 min; (C) with 20 wt.% for C_{CTAC} and t = 30 min; (D) with 5 wt.% for C_{CTAC} and without sonofragmentation.*

From the optimized formulation B (Figure 3), we evaluate a sizing procedure for CFRP as shown in Figure 6. This figure demonstrates the influence of the PEKK oligomer sizing on the fiber/matrix interface. The Figure 6 (A) shows a discontinuity between the matrix and fiber which is characterized by a delamination in unsized CFRP. This

adhesion is characterized by the attachment of the polymer matrix during the cryocut represent Figure 6 (B). This figure shows interest of PEKK sizing in matrix/fiber interface. This interface result is demonstrated with same sizing agent in PEEK matrix [11].

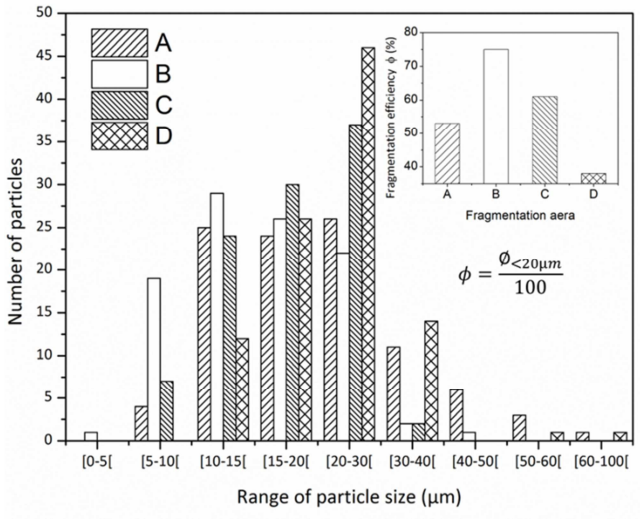

Figure 5. *Histogram of particle size ranges and fragmentation efficiency, ϕ, calculated for: (A) without C_{CTAC}; (B) with 2 wt.% for C_{CTAC} and t = 30 min; (C) with 20 wt.% for C_{CTAC} and t = 30 min; (D) with 5 wt.% for C_{CTAC} and without sonofragmentation*

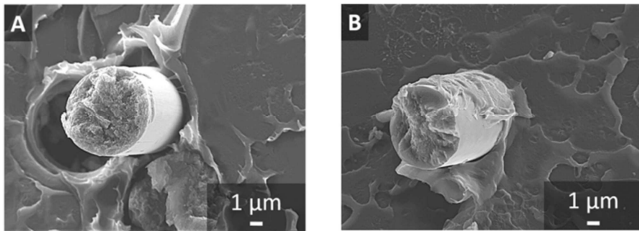

Figure 6. *Scanning electron microscopy of cryocut of CRFP; (A) is composite reinforced on unsized carbon fiber and (B) is composite reinforced on carbon fiber sized by PEKK oligomer*

5. Conclusion

This study led to the development of a methodology for the characterization and optimization of aqueous thermoplastic polymer dispersions, directly in solution, by the study of their destabilization velocity. The use of analytical centrifugation allowed the characterization of 40 samples subjected to a process of sonofragmentation, for which 7 experimental parameters were controlled. The application of a QSPR methodology with artificial neural networks allowed 2 experimental parameters to be identified as strongly connected to the destabilization velocity of the formulations, after sonofragmentation. By controlling only these 2 parameters (mass concentration of surfactant and duration of sonication), it was possible to define a design space for sonofragmentation with another thermoplastic polymers class, showing that the model was valid for PEKK family.

Within this design space, 4 zones were studied by scanning electron microscopy and image analysis. These analyses showed that the process of sonofragmentation could be optimized by modulating the mass concentration of surfactant and the duration of sonication. The yield of sonofragmentation was calculated for the 4 zones and showed a direct relationship with the results obtained by measuring the destabilization velocity of the dispersions. The analysis also showed that the destabilization velocity of the dispersion was connected to *Ds* and the number of particles with *Ps* < 20 µm.

The analysis of sonofragmentation images showed that the process was accompanied by an increase in the number of small particles with *Ps* < 5 µm. Particles with *Ps* < 20 µm made up the majority in the samples with high sonofragmentation yield. In all the samples, the presence of particles with *Ps* > 30 µm mixed with small particles explains the difficulty of precisely measuring *Ps* by PCS. In the case of complex formulations of polymers, the use of analytical centrifugation (LUMiFuge®) to determine the destabilization velocity of the dispersions can be useful. With this process, it is possible to study very complex granulometric profiles, directly in solution. The development of a QSPR study allowed the samples to be classified and notably reduced the number of experiments needed to obtain a design space displaying the optimized zones of sonofragmentation. The interest of this work is sustained by the potential of PEKK stable suspension for the processing of PEKK based materials used in a green sizing process. The novelty of this method is obtaining a PEKK stable suspension with formulation process without organic solvent.

Thanks to realization of cryocut on polymer composite PEKK/CF with carbon fiber sized and un-sized, this study demonstrate the influence of thermoplastic sizing on matrix/fiber interface. A Thermoplastic sizing with an optimized formulation improves adherence of matrix on fiber which involve a better mechanical performance.

Acknowledgements

The results of study were obtained in the context of the research project "COMPINNOV TP" at the IRT Saint Exupéry. Many thanks to the industrial and academic members of the IRT who supported this project through their contributions, both financial and in terms of specific knowledge:

Industrial members: AIRBUS OPERATIONS, ARIANE GROUP, AIRBUS GROUP INNOVATIONS, AIRBUS HELICOPTERS and THALES ALENIA SPACE.

Academic members: CIRIMAT, CNRS, ICA, IMRCP, ISAE and UPS.

Many thanks to the "Commissariat Général aux Investissements" and the "Agence Nationale de la Recherche" for their financial support in the framework of the "Programme d'Investissement d'Avenir" (PIA).

And finally, many thanks to Arkema group (France) for providing PEKK extractible fraction.

References

[1] Spyrou E. Thermoplastic powder coating. Hanover: Vincentz Network 2012.

[2] Sugama T, Webster R, Reams W, Gawlik K. High-performance polymer coatings for carbon steel heat exchanger tubes in geothermal environments. Journal of Materials Science 2000; 35: 2145-2154.

[3] DiMarzio D, Weizenecker C, Chu S, Anton D. Thermoplastic coating for composite structures. US 2005/0019501 A1, United States 2005.

[4] Normand B, Takenouti H, Keddam M, Liao H, Monteil G, Coddet CB. Electrochemical impedance spectroscopy and dielectric properties of polymer: application to PEEK thermally sprayed coating. Electrochimica Acta 2004; 49: 2981-2986.

[5] Li J, Liao H, Coddet C. Friction and wear behavior of flame-sprayed PEEK coatings. Wear 2002; 252: 824-831.

[6] Mahajan GV, Aher VS. Composite material: A review over current development and automotive application. International journal of scientific and research publications 2012; 2: 463-467.

[7] Joshi M, Chatterjee U. Polymer nanocomposite: an advanced material for aerospace. In Rana S, Fangueiro R, editors. Advanced Composite Materials for Aerospace Engineering. New Delhi: Elsevier 2016; 241-264

[8] Tian M, Tan H, Li H, You C. Molecular weight dependence of structure and properties of chitosan oligomers. RSC Advances. 2015; 5: 69445-69452.

[9] Lu Y, Larock RC. New Hybrid Latexes from a Soybean Oil-Based Waterborne Polyurethane and Acrylics via Emulsion Polymerization. Biomacromolecules 2007; 8: 3108-3114.

[10] Parmar R, Patel K, Parmar J. High-performance waterborne coatings based on epoxy-acrylic-graft-copolymer-modified polyurethane dispersions. Polymer International 2005; 54: 488-494.

[11] Giraud I, Franceschi-Messant S, Perez E, Lacabanne C, Dantras E. Influence of new thermoplastic sizing agents on the mechanical behavior of poly (ether ketone ketone)/carbon fiber composites. Journal of Applied Polymer Science 2013; 266: 94-99.

[12] Malho Rodrigues A, Franceschi S, Perez E, Garrigues J-C. Formulation optimization for thermoplastic sizing polyetherimide dispersion by quantitative structure–property relationship: experiments and artificial neural networks. Journal of Materials Science 2015; 50: 420–426. (2015).

[13] Yumitori S, Wang D, Jones F. The role of sizing resins in carbon fibre-reinforced polyethersulfone (PES). Composites 1994; 25: 698-705.

[14] Yuan H, Lu C, Zhang S, Wu G. Preparation and characterization of a polyimide coating on the surface of carbon fibers. New Carbon Materials 2015; 30: 115-121.

[15] Yuan H, Zhang S, Lu C. Surface modification of carbon fibers by a polyether sulfone emulsion sizing for increased interfacial adhesion with polyether sulfone. Applied Surface Science 2014; 317: 737-744.

[16] Liu WB, Zhang S, Hao LF, Jiao WC, Yang F, Li X. F et al. Properties of carbon fiber sized with poly (phthalazinone ether ketone) resin. Journal of Applied Polymer Science 2012; 6: 3702-3709.

[17] Singh S, Baghel RS, Yadav L. A review on solid dispersion. International Journal of Pharmacy and Life Sciences 2012; 2: 1078-1095.

[18] Martena V, Shegokar R, Di Martino P, Müller HR. Effect of four different size reduction methods on the particle size, solubility enhancement and physical stability of nicergoline nanocrystals. Drug development and industrial pharmacy 2014; 40: 1199-205 (2014).

[19] Hafshejani LD, Tangsir S, Koponen H, Riikonen J, Karhunen T, Tapper U, et al. Synthesis and characterization of Al2O3 nanoparticles by flame spray pyrolysis (FSP) — Role of Fe ions in the precursor. Powder Technology 2016; 298: 42-49.

[20] Turker M. Effect of production parameters on the structure and morphology of Ag nanopowders produced by inert gas condensation. Materials Science and Engineering A 2004; 367: 74-81.

[21] Kandasamy S, Sorna Prema R. Methods of synthesis of nano particles and its applications. Journal of Chemical and Pharmaceutical Research 2015; 7: 278-285.

[22] Prasad Yadav T, Manohar Yadav R, Pratap Singh D. Mechanical Milling: a Top Down Approach for the Synthesis of Nanomaterials and Nanocomposites. Nanoscience and Nanotechnology 2012; 2: 22-48 (2012).

[23] Nguyen T, He J. Preparation of titanium monoxide nanopowder by low-energy wet ball-milling. Advanced Powder Technology 2016; 27: 1868-1873.

[24] Rama Rao NV, Hadjipanayis GC. Influence of jet milling process parameters on particle size, phase formation and magnetic properties of MnBi alloy. Journal of Alloys and Compounds 2015; 629: 80-83.

[25] Patel CM, Chakraborty M, Murthy ZVP. Fast and scalable preparation of starch nanoparticles by stirred media milling. Advanced Powder Technology 2016; 27: 1287-1294.

[26] Marković S, Mitrić M, Starčević G, Uskoković D. Ultrasonic de-agglomeration of barium titanate powder. Ultrasonics Sonochemistry 2008; 15: 16-20.

[27] Guittonneau F, Abdelouas A, Grambow B, Huclier S. The effect of high power ultrasound on an aqueous suspension of graphite. Ultrasonics Sonochemistry 2010; 17: 391-398.

[28] Gopi KR, Nagarajan R. Application of Power Ultrasound in Cavitation Erosion Testing of Nano-Ceramic Particle/Polymer Composites. Solid State Phenomena 2008; 136: 191-204.

[29] Mizushima Y, Nagami Y, Nakamura Y, Saito T. Interaction between acoustic cavitation bubbles and dispersed particles in a kHz-order-ultrasound-irradiated water. Chemical Engineering Science 2013; 93: 395-400.

[30] Yang Y-J, Kelkar AV, Zhu X, Bai G, Ng HT, Corti DS, et al. Effect of sodium dodecylsulfate monomers and micelles on the stability of aqueous dispersions of titanium dioxide pigment nanoparticles against agglomeration and sedimentation. Journal of Colloid and Interface Science 2015; 450: 434-445.

[31] Goyal N, Rastogi D, Jassal M, Agrawal AK. Chitosan as a potential stabilizing agent for titania nanoparticle dispersions for preparation of multifunctional cotton fabric. Carbohydrate Polymers 2016; 154: 167-175.

[32] Hsiao B S, Gardner K H. Polymorphism and crystal structure identification in poly (aryl ether ketone ketone)s. Macromolecular Chemistry and Physics 1996; 197: 185-213.

[33] Raman V, Abbas A. Experimental investigations on ultrasound mediated particle breakage. Ultrasonics Sonochemistry 2008; 15: 55-64.

[34] Le T, Epa VC, Burden FR, Winkler DA. Quantitative Structure–Property Relationship Modeling of Diverse Materials Properties. Chemical Reviews 2012; 122: 2889-2919.

[35] Hammett LP. Some Relations between Reaction Rates and Equilibrium. Chemical Reviews 1935; 17: 125-136.

[36] Taft RW. Polar and Steric Substituent Constants for Aliphatic and o-Benzoate Groups from Rates of Esterification and Hydrolysis of Esters 1. Journal of the American Chemical Society 1952; 74: 3120-3128.

[37] Hansch C, Fujita T. p -σ-π Analysis. A Method for the Correlation of Biological Activity and Chemical Structure. Journal of the American Chemical Society 1964; 86: 1616-1626.

[38] Free SM, Wilson JW. A Mathematical Contribution to Structure-Activity Studies. Journal of Medicinal Chemistry 196; 7: 395-399.

[39] Broderick S, Rajan K. Informatics derived materials databases for multifunctional properties. Science and Technology of Advanced Materials 2015; 16: 013501.

[40] Hiller S, Glaz A, Rastrigin L, Rosenblit A. Recognition of physiological activity of chemical compounds on perceptron with random adaptation of structure. Dokl Akad Nauk SSSR 1971; 199: 851-853.

[41] Rumelhart DE, Hinton GE, Williams RJ. Learning representations by back-propagating errors. Nature 1986; 323: 533-536.

[42] Pai TY, Tsai YP, Lo HM, Tsai CH, Lin CY. Grey and neural network prediction of suspended solids and chemical oxygen demand in hospital wastewater treatment plant effluent. Computers & Chemical Engineering 2007; 31: 1272-1281.

[43] Pai TY, Yang PY, Wang SC, Lo MH, Chiang CF, Kuo, JL, et al. Predicting effluent from the wastewater treatment plant of industrial park based on fuzzy network and influent quality. Applied Mathematical Modelling 2011; 450: 434-445.

[44] Ochoa-estopier LM, Jobson M, Smith R. Operational optimization of crude oil distillation systems using artificial neural networks. Computers & Chemical Engineering 2013; 59: 178-185.

[45] Verma S, Sharma A, Sharma S, Priyadarshi RK. Modeling of trihalomethanes (THMS) in drinking water by artificial neural network. Pollution Research 2011; 30: 7-11.

[46] Braga CC, Dias MS. Application of Neural Networks for unfolding neutron spectra measured by means of Bonner Spheres. Nuclear Instruments and Methods in Physics Research Section A 2002; 476: 252-255.

[47] Zheng XM, Zubal IG, Seibyl JP, King MA. Correction for Crosstalk Contaminations in Dual Radionuclide ^{99m}Tc and ^{123}I Images Using Artificial Neural Network. IEEE Transactions on Nuclear Science 2004; 51: 2649-2653.

[48] King D, Lyons WB, Flanagan C, Lewis E. An optical fibre ethanol concentration sensor utilizing Fourier transform signal processing analysis and artificial neural network pattern recognition. Journal of Optics A: Pure and Applied Optics 2003; 5: S69–S75.

[49] Prouillac C, Vicendo P, Garrigues J-C, Poteau R, Rima G. Evaluation of new thiadiazoles and benzothiazoles as potential radioprotectors: Free radical scavenging activity in vitro and theoretical studies (QSAR, DFT). Free Radical Biology and Medicine 2009; 46: 1139-1148.

[50] Frisken BJ. Revisiting the method of cumulants for the analysis of dynamic light-scattering data. Applied Optics 2001; 40: 4087.

[51] Berne BJ, Pecora R. Dynamic Light Scattering with Applications to Chemistry, Biology, and Physics. New York: John Wiley & Sons, Inc 1977.

[52] Mukerjee P, Mysels KJ. Critical Micelle Concentrations of Aqueous Surfactant Systems. Washington: National Bureau of Standards 1971.